AFRL-AFOSR-VA-TR-2018-0310

Stochastic Models for cold sprayed microstructures

Francois Willot
Ass Recherche Devel Methode Proces Indus

07/31/2018
Final Report

Air Force Research Laboratory
AF Office Of Scientific Research (AFOSR)/ RTB1
Arlington, Virginia 22203
Air Force Materiel Command

DISTRIBUTION A: Distribution approved for public release.

REPORT DOCUMENTATION PAGE

Form Approved
OMB No. 0704-0188

1. REPORT DATE *(DD-MM-YYYY)*	2. REPORT TYPE	3. DATES COVERED *(From - To)*
14-12-2017	Final Technical	15/09/2015 to 15/09/2017

4. TITLE AND SUBTITLE
Stochastic Models for Cold Sprayed Microstructures

5a. CONTRACT NUMBER

5b. GRANT NUMBER
FA9550-15-1-0461 DEF

5c. PROGRAM ELEMENT NUMBER

6. AUTHOR(S)
Willot, François
Bortolussi, Vincent
Jeandin, Michel
Figliuzzi, Bruno
Faessel, Matthieu

5d. PROJECT NUMBER

5e. TASK NUMBER

5f. WORK UNIT NUMBER

7. PERFORMING ORGANIZATION NAME(S) AND ADDRESS(ES)
Centre for Mathematical Morphology
Dept. of Mathematics
35 rue St Honore
77300 Fontainebleau, France

8. PERFORMING ORGANIZATION REPORT NUMBER

9. SPONSORING/MONITORING AGENCY NAME(S) AND ADDRESS(ES)
AFOSR
875 N. Randolph St.,
RM 3112
Arlington, VA 22203-1954

10. SPONSOR/MONITOR'S ACRONYM(S)

11. SPONSOR/MONITOR'S REPORT NUMBER(S)

12. DISTRIBUTION/AVAILABILITY STATEMENT
Distribution A - Approved for Public Release

13. SUPPLEMENTARY NOTES

14. ABSTRACT

We study the microstructure of cold sprayed films of copper particles deposited onto a carbon fiber reinforced polymer. The microstructure of the coating is made of a packing of seemingly round-shaped particles of varying sizes embedded in a polymer matrix. The copper particles are separated by thin interstices. The coating is designed to cover the body of recent commercial aircrafts. Its role is to protect the aircraft from lightning impact by ensuring that the surface is conductive enough to evacuate electrical charges. A high resistivity contrast is observed between the copper particles and the polymer matrix. Therefore, the global resistivity of the material is highly dependent on the microstructure geometry. Following an approach commonly used in materials science, to investigate its influence on the electrical properties of the global material at the macroscopic scale, we design a 3D multiscale stochastic model that enables us to simulate the microstructure. The model is based upon a generalization of the classical Johnson-Mehl tessellation, which accounts for the interstices that appear between copper particles. The method is very general and could potentially be applied to model any microstructure exhibiting similar interstices between aggregates of particles.

15. SUBJECT TERMS
Colspray, models of random structures, stochastic geometry, stereology

16. SECURITY CLASSIFICATION OF:			17. LIMITATION OF ABSTRACT	18. NUMBER OF PAGES	19a. NAME OF RESPONSIBLE PERSON
a. REPORT	b. ABSTRACT	c. THIS PAGE			François Willot
U	U	U	U		19b. TELEPHONE NUMBER *(Include area code)* +33 16469 4807

Reset

Standard Form 298 (Rev. 8/98)
Prescribed by ANSI Std. Z39.18
Adobe Professional 7.0

INSTRUCTIONS FOR COMPLETING SF 298

1. REPORT DATE. Full publication date, including day, month, if available. Must cite at least the year and be Year 2000 compliant, e.g. 30-06-1998; xx-06-1998; xx-xx-1998.

2. REPORT TYPE. State the type of report, such as final, technical, interim, memorandum, master's thesis, progress, quarterly, research, special, group study, etc.

3. DATES COVERED. Indicate the time during which the work was performed and the report was written, e.g., Jun 1997 - Jun 1998; 1-10 Jun 1996; May - Nov 1998; Nov 1998.

4. TITLE. Enter title and subtitle with volume number and part number, if applicable. On classified documents, enter the title classification in parentheses.

5a. CONTRACT NUMBER. Enter all contract numbers as they appear in the report, e.g. F33615-86-C-5169.

5b. GRANT NUMBER. Enter all grant numbers as they appear in the report, e.g. AFOSR-82-1234.

5c. PROGRAM ELEMENT NUMBER. Enter all program element numbers as they appear in the report, e.g. 61101A.

5d. PROJECT NUMBER. Enter all project numbers as they appear in the report, e.g. 1F665702D1257; ILIR.

5e. TASK NUMBER. Enter all task numbers as they appear in the report, e.g. 05; RF0330201; T4112.

5f. WORK UNIT NUMBER. Enter all work unit numbers as they appear in the report, e.g. 001; AFAPL30480105.

6. AUTHOR(S). Enter name(s) of person(s) responsible for writing the report, performing the research, or credited with the content of the report. The form of entry is the last name, first name, middle initial, and additional qualifiers separated by commas, e.g. Smith, Richard, J, Jr.

7. PERFORMING ORGANIZATION NAME(S) AND ADDRESS(ES). Self-explanatory.

8. PERFORMING ORGANIZATION REPORT NUMBER. Enter all unique alphanumeric report numbers assigned by the performing organization, e.g. BRL-1234; AFWL-TR-85-4017-Vol-21-PT-2.

9. SPONSORING/MONITORING AGENCY NAME(S) AND ADDRESS(ES). Enter the name and address of the organization(s) financially responsible for and monitoring the work.

10. SPONSOR/MONITOR'S ACRONYM(S). Enter, if available, e.g. BRL, ARDEC, NADC.

11. SPONSOR/MONITOR'S REPORT NUMBER(S). Enter report number as assigned by the sponsoring/ monitoring agency, if available, e.g. BRL-TR-829; -215.

12. DISTRIBUTION/AVAILABILITY STATEMENT. Use agency-mandated availability statements to indicate the public availability or distribution limitations of the report. If additional limitations/ restrictions or special markings are indicated, follow agency authorization procedures, e.g. RD/FRD, PROPIN, ITAR, etc. Include copyright information.

13. SUPPLEMENTARY NOTES. Enter information not included elsewhere such as: prepared in cooperation with; translation of; report supersedes; old edition number, etc.

14. ABSTRACT. A brief (approximately 200 words) factual summary of the most significant information.

15. SUBJECT TERMS. Key words or phrases identifying major concepts in the report.

16. SECURITY CLASSIFICATION. Enter security classification in accordance with security classification regulations, e.g. U, C, S, etc. If this form contains classified information, stamp classification level on the top and bottom of this page.

17. LIMITATION OF ABSTRACT. This block must be completed to assign a distribution limitation to the abstract. Enter UU (Unclassified Unlimited) or SAR (Same as Report). An entry in this block is necessary if the abstract is to be limited.

François Willot
Mines ParisTech
Centre for Mathematical Morphology
35 rue Saint Honoré
F-77300 Fontainebleau
France
Email: francois.willot@ensmp.fr

Monique Williams
AFOSR
AF Office of Scientific Research
CC: Prof. Ali Sayir

Fontainebleau, France, March 20, 2018

Dear Business office,

Please find enclosed with this submission the final report for grant FA9550-15-1-0461 titled "Stochastic Models for Cold Sprayed Microstructures". The report is on pages 1-14. Pages 15 to 21 is a copy of a conference proceeding by V. Bortolussi, F. Borit, A. Chesnaud, M. Jeandin, M. Faessel, B. Figliuzzi, F. Willot, K. Roche, G. Surdon (2016) titled "Cold spray of metal-polymer composite coatings onto Carbon Fiber-Reinforced Polymer (CFRP), Proceedings of the International Thermal Spray Conference (ITSC), Shangai (China) 324, 26. An article is currently under review in the journal Image Analysis & Stereology.

Also enclosed is a copy of form SF 298, as per your request.

Very respectfully,

François Willot

Stochastic Models for cold sprayed microstructures

VINCENT BORTOLUSSI, PHD[1], BRUNO FIGLIUZZI, PHD[2], FRANÇOIS WILLOT, PHD[2], MATTHIEU FAESSEL, PHD[2] AND MICHEL JEANDIN, PROF.[1]

[1]Centre for Materials Engineering, Mines ParisTech - PSL Research University, Evry, F-91003, France, [2]Centre for Mathematical Morphology, Mines ParisTech - PSL Research University, Fontainebleau, 77300, France

e-mail: bruno.figliuzzi@mines-paristech.fr

(Submitted)

ABSTRACT

In this article, we study the microstructure of cold sprayed films of copper particles deposited onto a carbon fiber reinforced polymer. The microstructure of the coating is made of a packing of seemingly round-shaped particles of varying sizes embedded in a polymer matrix. The copper particles are separated by thin interstices. The coating is designed to cover the body of recent commercial aircrafts. Its role is to protect the aircraft from lightning impact by ensuring that the surface is conductive enough to evacuate electrical charges. A high resistivity contrast is observed between the copper particles and the polymer matrix. Therefore, the global resistivity of the material is highly dependent on the microstructure geometry.
Following an approach commonly used in materials science, to investigate its influence on the electrical properties of the global material at the macroscopic scale, we design a 3D multiscale stochastic model that enables us to simulate the microstructure. The model is based upon a generalization of the classical Johnson-Mehl tessellation, which accounts for the interstices that appear between copper particles. The method is very general and could potentially be applied to model any microstructure exhibiting similar interstices between aggregates of particles.

Keywords: Colspray, microstructure simulation, mathematical morphology, stochastic geometry, stereology.

INTRODUCTION

Modern materials manufacturing has evolved toward a better control and optimization at the microscopic scale. Hence, microstructures commonly exhibit complex morphologies mixing various materials including carbon fibers arrangements into polymer matrix. The physical and mechanical features of heterogeneous materials at the macroscopic scale are largely dictated by phenomena appearing at the microscopic level. Therefore, the development of numerical tools deriving the physical properties of a material at the macroscopic scale from its geometry at the microscopic scale has been a very active topic of research over the past few years [28].

Current computational capabilities and imaging techniques can fill the gap between microstructure observation and computation of effective physical and mechanical properties through simulation. However, if recent tomography processes can entirely recreate complex microstructures, some materials remains inadapted to imaging process involving high energy beams. In this case, an alternative is to rely on stochastic models to describe and simulate microstructures. Computational tools and models brought by mathematical morphology [25, 27] allow to generate and simulate complex microstructures on which one can perform physical simulations [30]. This method can cope very well with multiscale and multiphased random sets [17], as demonstrated by recent studies investigating the effects of rigid fillers into soft matrix such as black carbon particles embedded into a polymer matrix [15, 13] or shells of argan nut in polypropylene [9]. Recently, similar methods were used to describe polycristalyne microstructures [14].

In this study, our aim is to simulate the electrical properties of a biphased coating obtained by thermal spraying. The coating is designed to cover the body of recent commercial aircrafts. Its role is to protect the aircraft from lightning impact by ensuring that the surface is conductive enough to evacuate electrical charges. Numerous physical and mechanical properties of cold sprayed coatings have already been investigated in the literature, including oxidation [7], Young's Modulus [2], porosity [3] or thermal conductivity [5]. Jeandin et *al.* [16] presented a model of coating build up in plasma spray. More recently, Delloro et *al.* [8] developed a morphological model for the cold spray process that accounts for the morphology of the deposit and for mechanical, physical and dynamic phenomena. However, to our knowledge, this study constitutes one of the first attempt to model the electrical properties of cold spray deposits from their microstructure.

In this paper we present a 3D stochastic model describing the coating microstructure. The model is derived from experimental images of slices of the

material taken with a microscope. The microstructure is constituted of copper particles embedded in a PEEK polymer matrix. The particles are separated by thin interstices of PEEK polymer. In terms of resistivity, a high constrast prevails between the polymer and the copper particles. Hence, a key issue toward an effective modeling of the microstructure is to accurately reproduce the interstice thicknesses and repartition. To that end, we introduce a new stochastic model derived from the classical Johnson-Mehl tessellation [18, 20, 21, 22] that enables us to properly reproduce these geometrical characteristics. The method is very general and could potentially be applied to model any microstructure exhibiting similar interstices between aggregates of particles.

The article is organized as follows. In section 2, we describe the materials on which we conduct our study and we briefly recall the basics of cold spray deposition. In section 3, we discuss the segmentation techniques and the statistical features used to process the experimental microscopic images. The 3D stochastic model is described in section 4, and we comment on the results of the study in section 5. Conclusions are drawn in the last section.

MATERIALS

MATERIALS

The body of recent commercial aircrafts is made of carbon fiber-reinforced polymers. These materials ensure high mechanical properties while being lighter than regular aluminium alloys. However, the polymer matrix is generally highly electrically insulating, which causes security concerns with lightning. Higher-grade aerospace composites are made with a matrix of PEEK (Poly-Ether-Ether-Ketone), a thermoplastic polymer offering good mechanical and thermal properties. In addition the PEEK is a very good insulator with a resistivity of $1.0 \times 10^{14}\,\Omega\,\mathrm{m}$.

To evacuate electrical charges in case of lightning impact, a mesh of copper is ordinary applied onto the composite body. Copper is a readily available electrical conductor, that is easily machinable and corrosion resistant. The electrical resistivity of copper is $1.68 \times 10^{-8}\,\Omega\,\mathrm{m}$.

To avoid complex manufacturing and assembly of copper meshings, we developed a new coating method which relies on copper powder thermally sprayed onto composite parts. More precisely, to achieve an adherent and electrically conductive layer we use a powders mixture. The mixture contains 80% volumetric of spherical copper powder (10-35 µm) and 20% of irregular PEEK particles (35-65 µm), increasing adherence with the composite. The mixture is sprayed using the cold-gas dynamic spraying or "cold spray" process.

PROCESS

Cold spray is a thermal spraying process using high speed spraying of powders to create a dense coating. It relies on a gas flow to drive the powder toward the substrate. The gas is usually nitrogen under pressure (1 to 4 MPa), which is heated (200 to 800°C) and accelerated through a convergent-divergent (De Laval type) nozzle. The powder is injected in the accelerated gas flow and can reach supersonic speed. Due to relatively low spraying temperature and processing time, powder particles remain solid. When powder particles impact the substrate, both of them undergo plastic strain. The adhesion of the coating is usually guaranteed by mechanical and chemical bonding. This process can lead to very dense coating due to dynamic impact, as well as low oxide content due to low temperature. In this study, we use manufactured coating made of a copper and PEEK mixture to investigate the microstructure of cold spray coatings.

Samples preparation

Cold spray coatings were cross-sectioned and polished previous to observation. Coating samples were cut in two directions, along the spraying path and orthogonal to the spraying path. Cutting and polishing debond copper particles due to poor mechanical anchorage in the matrix, leaving dark holes at the surface. Manual polishing severely influences debonding phenomenon. Samples were then metallized with a 2 nm layer of Gold-Palladium using a Cressington sputter coater. This is a key operation as the layer modifies the colour of the PEEK matrix, by greatly enhancing colour gradient between phases. We observed cross-sections at x20 magnification in bright field using a Leica optical microscope with a resolution of 0.2428 µm per pixel. The selected observation scale was chosen to obtain a representative fraction of copper while highlighting PEEK interstices.

Microstructure

The microstructure of the coating can be observed in Fig. 1 with copper particles in yellow, dark footprints and a grey matrix of PEEK. The resulting cold spray coating contains copper particles embedded in a PEEK matrix. The matrix is obtained from irregular PEEK particles highly deformed upon high speed impact. It is considered dense with no pores appearing at this scale. Copper particles are deforming solely when impacting each other resulting in a limited

plastic strain. These particles are forming a network of copper clusters.

Common cold spraying of metal particles onto metal substrate generally involve chemical bonding and interdiffusion at the interfaces between particles and substrate. In our case, optical observation at larger scale highlights thin ($<10\,\mu m$) PEEK layers lying between deformed copper particles, as shown in Fig. 2. These interstices prevent direct contact between copper particles. Filled with electrically insulating PEEK, they allegedly increase resistivity, thus lowering the coating conductivity.

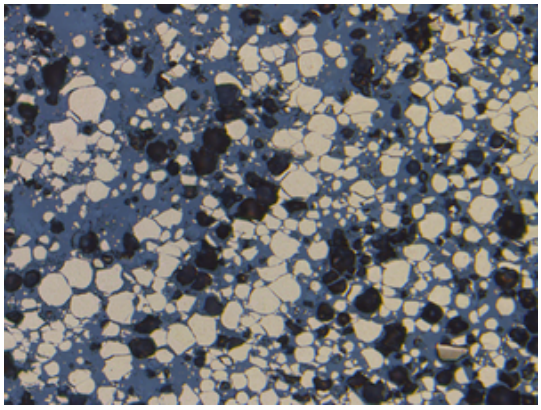

Fig. 1: Optical microscope cross-section of the coating microstructure with debonded particles in black (2560×1920 pixels equals to $620 \times 476\,\mu m^2$)

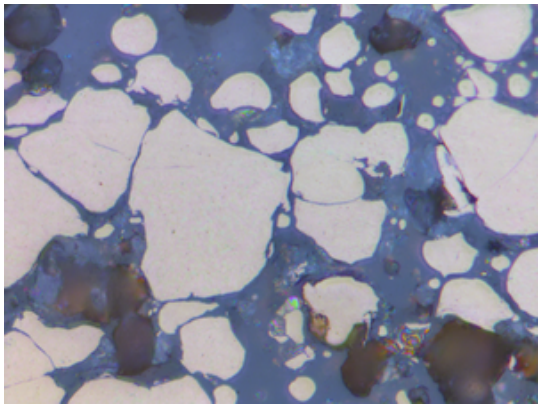

Fig. 2: Magnified optical microscope cross-section of the microstructure of the coating

IMAGE SEGMENTATION AND CHARACTERIZATION

In this section, we describe the segmentation process developed for the images of the microstructure of the coating.

SEGMENTATION PROCESS

The segmentation process is performed with a Python script based upon the free image library SMIL [11]. It aims at identifying the two phases of the material, namely the PEEK matrix and the copper aggregates. Previous to any segmentation operation, we transform the RGB-images from the microscope into 8-bits images, by extracting the second channel, as shown in Fig. 3a. Then, we threshold the image with an automatic Otsu [23] process involving two thresholds. This leads to three-phased coloured images, as shown in Fig. 3b, where copper particles appear in yellow, footprints of the debonded particles in black and the PEEK matrix in red. Due to low greylevel gradient, this first thresholding operation is not able to separate all close particles.

In a second step, we merge the footprints into the matrix by thresholding the particles (Fig. 3c). Next, small isolated particles and observation artefacts with an area smaller than 100 pixels are removed. Then we select inner markers for the particles with by keeping the h-maxima of a distance function applied on the particles. This operation can be seen on Fig. 3d and the result on Fig. 3e.

Once the markers are selected, particles are separated with a watershed process [4, 29], using the core of the particles and a grey scale colour gradient map to define the boundaries of each cell. Separation achieved with the watershed process is assessed on Fig. 3f. Finally we label each particles obtained after the watershed. The watershed process is able to achieve good separation of close particles, even if the interstices do not always appear on thresholded images. The main steps depicted on Fig. 3 use smaller images than the real samples.

The same exact process is applied on debonded particles. This time real particles are merged into the matrix, and footprints are filled by changing pixels values of thresholded images (Fig. 4a and Fig. 4b). As one footprint could have contained several particles, this filling process is not able to reconstruct hypothetical interstices separating them. Then we apply the segmentation process used on the particles to label the debonded particles, as shown in Fig. 4c and Fig. 4d.

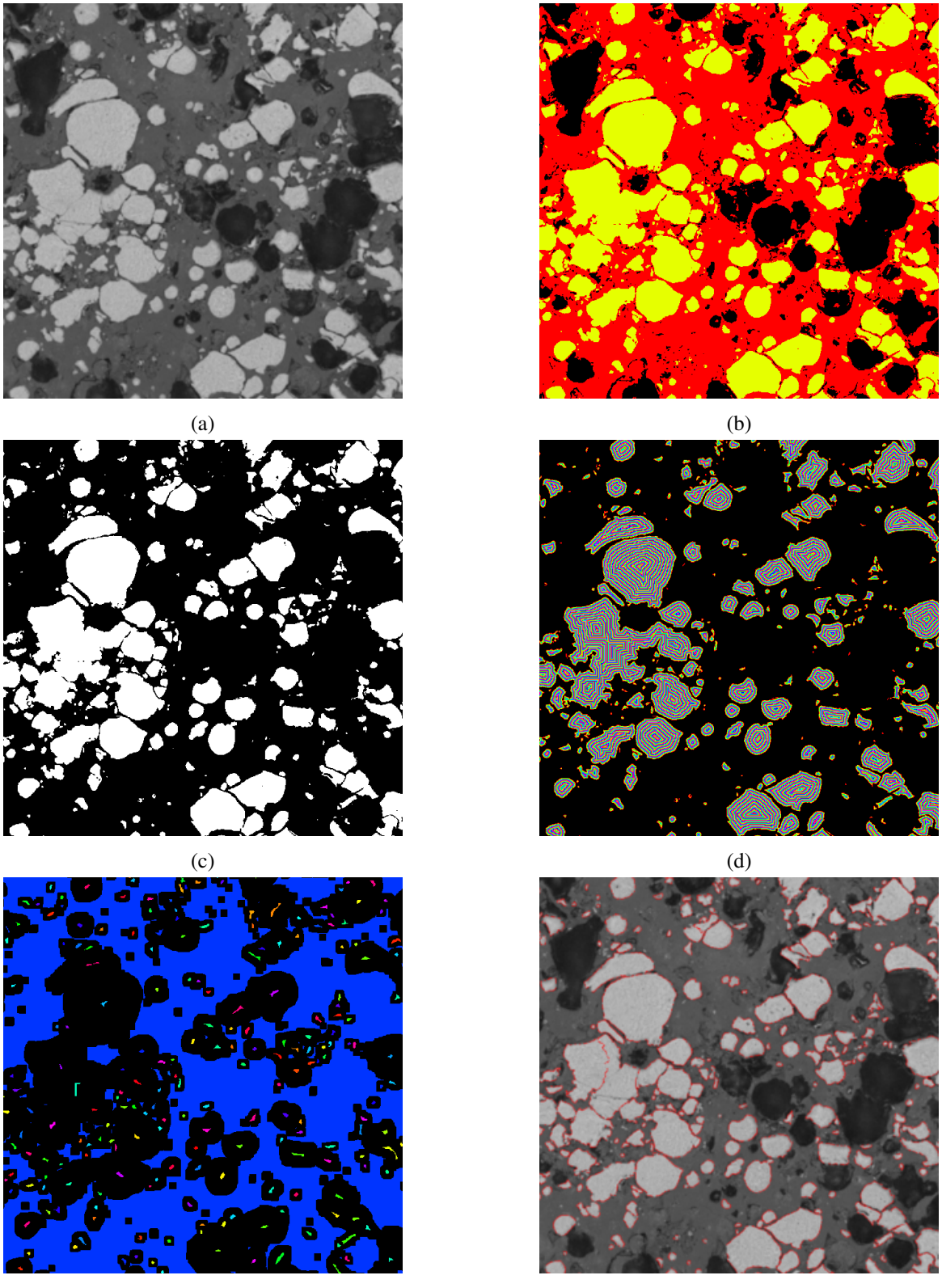

Fig. 3: Segmentation process of particles. (a) Grey scale image. (b) Thresholded image. (c) Particles selection. (d) Distance function on particles. (e) Cores of particles. (f) Watershed procedure on particles

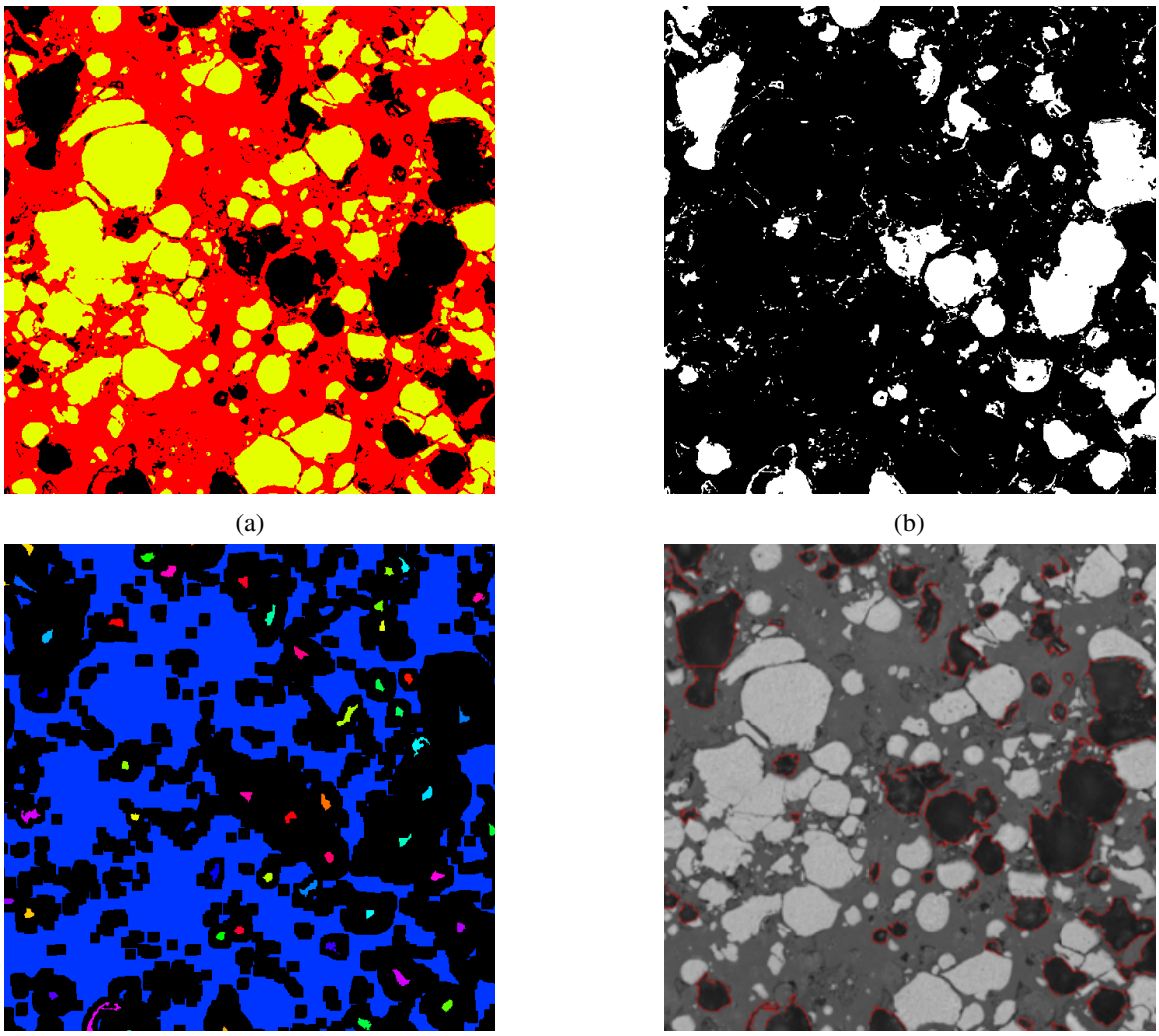

(a) (b)

(c) (d)

Fig. 4: Segmentation process of debonded particles. (a) Thresholded image. (c) Debonded particles selection. (d) Cores of debonded particles. (e) Watershed procedure on debonded particles

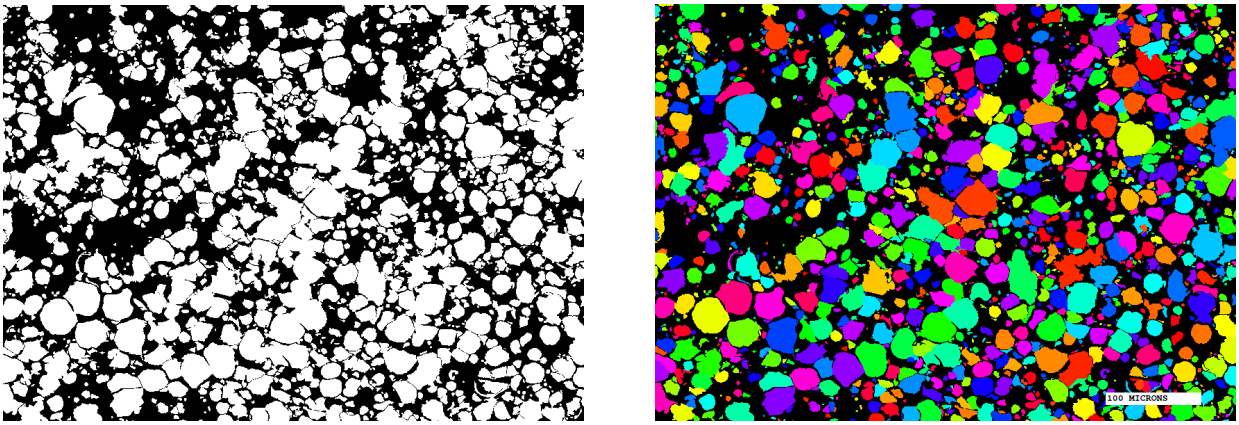

(a) (b)

Fig. 5: (a) Final binary image. (b) Labelled particles.

Finally we superimpose the two labelled images (Fig. 5b). By colouring the matrix in black and each particle in white we obtain a binary image like Fig. 5a, used for morphological measurements. The segmentation process was applied on 13 randomly-selected images of 2560×1960 pixels representing an area of $620\,\mu m^2 \times 476\,\mu m^2$.

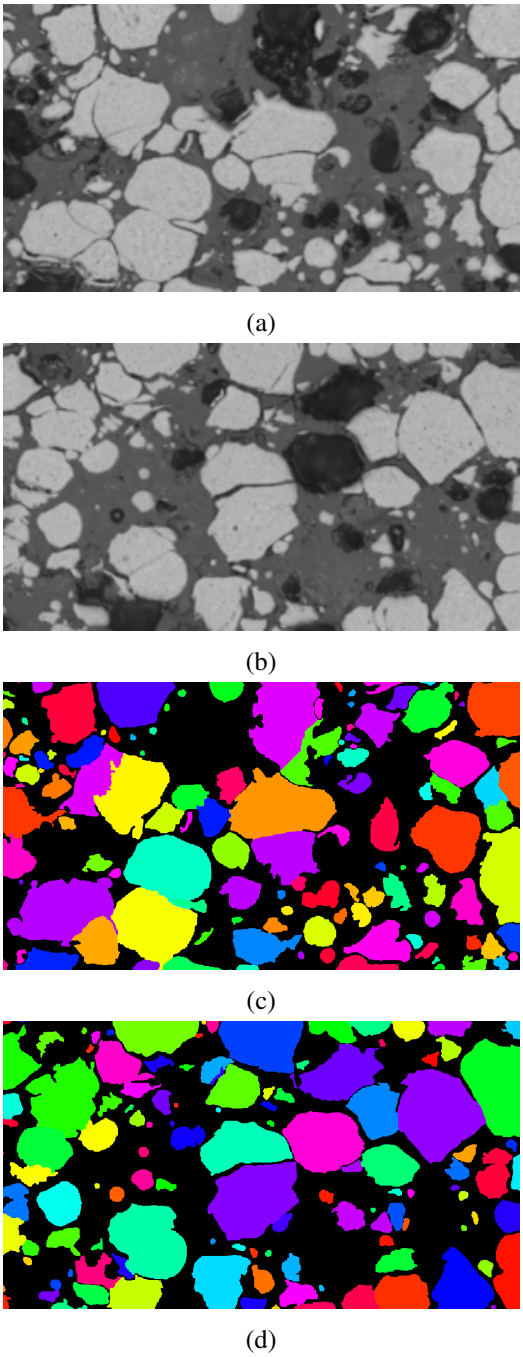

(a) (b) (c) (d)

Fig. 6: Separation of close particles. (a) and (b) Examples of close particles. (c) Separated particles without interstices. (d) Separated particles with interstices

MORPHOLOGICAL DATA

In this section, we conduct morphological measurements on the binary images to characterize the spatial distribution of copper particles. We focus more specifically on three morphological descriptions: the covariance, the granulometry and the thicknesses distribution of the interstices. These morphological measurements will be further exploited to compute the parameters of the microstructure model.

Covariance

The covariance is defined as the probability:

$$C(r) = P\{x \in \mathscr{H}, x+r \in \mathscr{H}\}, \qquad (1)$$

where $\mathscr{H}$ is the union of copper particles in the coating, x some point, and r some vector in $\mathbb{R}^2$.

For a stationary random set $\mathscr{H}$, the covariance does not depends on x anymore but only on r. It depends on the orientation and on the modulus of r and represents the probability for two points separated by distance r to belong to the same phase of the material. For $r = 0$, the covariance is equal to the surface fraction of $\mathscr{H}$ (in 2D). At large distance $|r| \gg 1$ the two events $x \in \mathscr{H}$ and $x+r \in \mathscr{H}$ become uncorrelated and $C(r = \infty) \approx C(0)^2$.

In this study, the covariance is measured for vectors of increasing moduli along the horizontal and vertical directions. Note that if the microstructure is isotropic, the covariance does not depend on the orientation of r. In our case, isotropy and stationarity have been assessed using all sample images. Fig. 7 shows the covariances measured on the segmented image represented in Fig. 1.

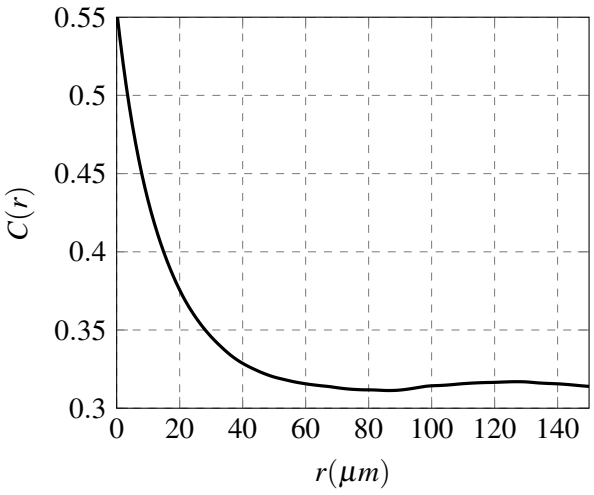

Fig. 7: Covariance curve as measured on the microstructure displayed in Fig. 5a.

The covariances obtained on the sample microstructure images show small dispersion, with

a mean surface fraction of 55% and a standard deviation of 4.9%. We compared the mean covariances measured vertically, horizontally and diagonally on the segmented images.

Granulometry

The cumulative granulometry is calculated by opening the copper phase with probability

$$G(s) = \frac{P\{x \in \mathscr{H}\} - P\{x \in \mathscr{H}(S;s)\}}{P\{x \in \mathscr{H}\}}, \qquad (2)$$

where x is a point in the image, $\mathscr{H}$ is the copper phase and $\mathscr{H}(S;s)$ is the morphological opening of $\mathscr{H}$ by a structural element S dilated by size s. In this case the structuring element is a 8-connexity square. The cumulative granulometry is measured on each image, giving a mean granulometry. However due to limited interstices segmentation, the measured granulometry does not completely reflect the real granulometry of the microstructure. In addition, it is important to note that the latter is different from the initial powder's granulometry because of the spraying process: some of the particles bounce at impact, thus missing in the microstructure. In addition, particules deform upon impact.

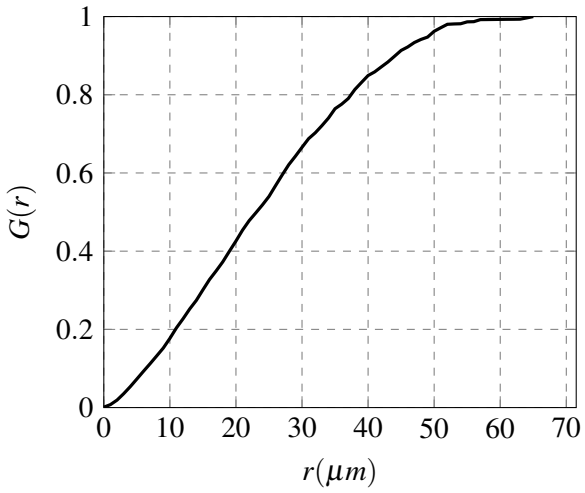

Fig. 8: Granulometry curve as measured on Fig. 5a.

Fig. 8 shows the granulometry as measured on the segmented image shown in Fig. 1. The mean cumulative granulometry shows that 10% of the microstructure is removed after an opening of size 1.7 µm ($\simeq$ 7 pixels), 50% of the microstructure is removed after an opening of size 5.7 µm ($\simeq$ 24 pixels) and 90% of the microstructure is removed after an opening of size 10.6 µm ($\simeq$ 44 pixels). When measured on the thirteen samples, it is less dispersed compared to the covariance.

Interstice thickness

Interstices appearing between copper particles are a key feature of the microstructure that strongly impact the conductivity of the material at the macroscopic scale. Therefore, they must be carefully described.

The labelled image issued from the segmentation process enables us to determine the number of non-connected particles n_0. After a dilation of 1 pixel, subtraction of the number of remaining isolated particles n_1 to the initial quantity gives the number of particles separated by a distance of 2 pixel: $n_{interstice} = n_0 - n_1$. Actually this process only measure distance of an even number of pixels. This method is repeated for 20 dilations on all sample images, thus yielding the size distribution of the interstices thickness.

We apply the interstices measuring process to obtain the thickness distribution displayed on Fig. 9.

The average distribution is fitted with an exponential law. The probability density function of this distribution is:

$$p(x,k) = ke^{-xk} \qquad (3)$$

The exponential law with k =1.19 µm^{-1} displayed on Fig. 10 shows good agreement with the experimental measurements. Interstices thickness were also measured on magnified images, showing similar distribution.

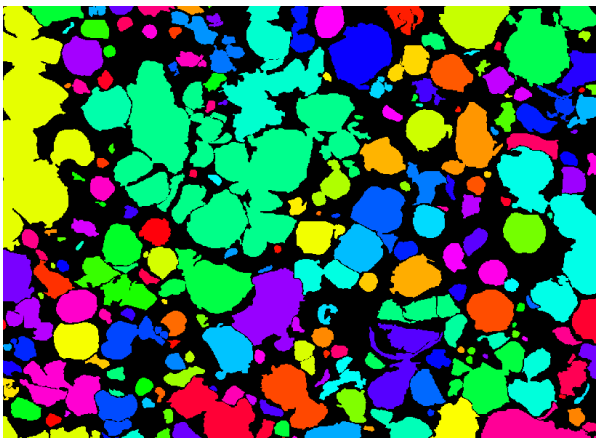

(a)

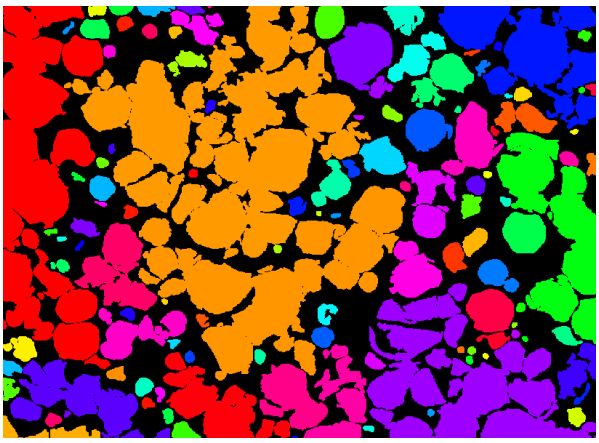

(b)

Fig. 9: Interstices measurement process on a quarter of an image. (a) Initial labelled particles. (b) Labelled particles after 2 dilation

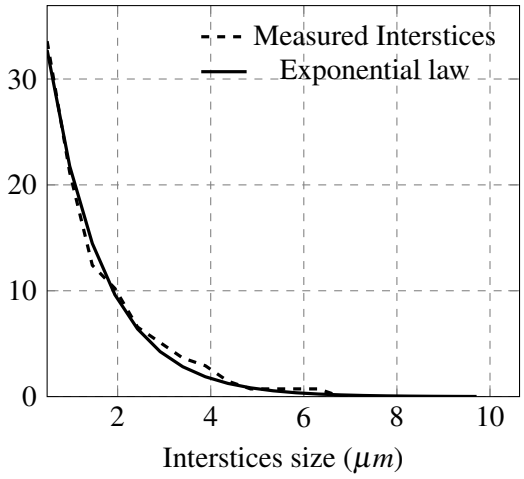

Fig. 10: Interstices mean thickness distribution

Copper phase perimeter and area

The perimeter of the copper phase can be roughly estimated by eroding the copper particles using a 8-connexity square of size one and considering the residue from the initial copper particles. Enclosure of the particles remains with a thickness of one pixel. An area measurement of the enclosure yields the perimeter of the particles per unit area. The perimeter is very sensitive to the segmentation of the interstices. The area is equal to $C(0)$, C being the covariance.

For experimental samples that have been cut in directions parallel to the covered substrate, the measurements yield a mean perimeter per unit area of $0.19\,\mu m^{-1}$ for the copper phase with a standard deviation of $0.01\,\mu m^{-1}$. The mean area of the copper phase is 0.55 with a standard deviation of 0.056. For experimental samples that have been cut in the vertical direction, the measurements yield a mean area for the copper phase of 0.59 with a standard deviation of 0.047.

STOCHASTIC MODEL FOR THE MICROSTRUCTURE

In this section, we introduce a probabilistic model for the 3D microstructures of the coating. We assume that the microstructure is described by copper spheres embedded in a PEEK matrix and separated by thin PEEK interstices. Covariance, copper fraction, granulometry, and interstice thickness are measured on 2D slices of the coating, thus 3D model's parameters must be inferred from these 2D informations. The final two-scale model relies on a two-step simulation process, namely 1/ Boolean spheres implantation of intensity θ, whose radii follow a Gamma distribution law with parameters λ and a; and 2/ Interstices implantation based on a modified Johnson-Mehl tessellation.

The boolean spheres represents copper particles, forming clusters due to interpenetration. Simulated volumes are sliced in 1000×1000 pixels images.

BOOLEAN MODEL OF SPHERES

We assume that the distribution of radii of the spheres is described by a Gamma law. The probability density function of the Gamma law is given by

$$p(r,\lambda,a) = \frac{r^{a-1}}{\Gamma(a)\lambda^a}\exp(-\frac{r}{\lambda}), \qquad (4)$$

where Γ denotes the Gamma function. The average radius of the spheres is $a\lambda$. Its variance is $a\lambda^2$.

We can easily show that the average surface of a grain is

$$S_v = \int_0^{+\infty} \frac{4\pi r^{a+1}}{\Gamma(a)\lambda^a}\exp(-\frac{r}{\lambda})\mathrm{d}r = 4\pi\lambda^2 a(a+1). \quad (5)$$

Similarly, the average volume of a grain is

$$V_v = \int_0^{+\infty} \frac{4\pi r^{a+2}}{3\Gamma(a)\lambda^a}\exp(-\frac{r}{\lambda})\mathrm{d}r = \frac{4\pi}{3}\pi\lambda^3 a(a+1)(a+2). \quad (6)$$

Let us denote by θ the intensity of the 3D Boolean model of spheres, and by θ_2 the intensity of the corresponding Boolean model of disk as observed on 2D slices extracted from the original model. To determine the 3D parameters of the model from the 2D measurements, we use the stereological formulae

$$\theta V_v = \theta_2 \bar{A} \qquad (7)$$

and

$$\theta S_v = \frac{4}{\pi}\theta_2 \bar{L}, \tag{8}$$

where $\bar{A}$ is the mean area of the sliced spheres and $\bar{L}$ their perimeter. We need to link the 2D measurements to the parameters of the boolean model. To that end, we rely on Miles' formulae [19, 6, 24]

$$\mathscr{A}_A = 1 - e^{(-\theta_2 \bar{A})} \tag{9}$$

and

$$\mathscr{L}_A = \theta_2 \bar{L}(1 - \mathscr{A}_A), \tag{10}$$

where $\mathscr{A}_a$ is the mean surface fraction of copper on the segmented images and $\mathscr{L}_A$ is the mean perimeter of the copper phase on the segmented images divided by the total surface.

Using Miles' formulae in conjunction with stereological formulae [6, 24], we find, for the Boolean model

$$\mathscr{A}_A = 1 - \exp(-\theta V_v), \tag{11}$$

and

$$\mathscr{L}_A = \theta \frac{\pi}{4} S_V \exp(-\theta V_v). \tag{12}$$

Overall, we have three unknowns in these equations, namely the intensity θ of the Boolean model and the parameters a and λ of the Gamma distribution. Hence, we can express all parameters as functions of a. Using (11) and (12), we find

$$\theta = -\frac{3}{4\pi\lambda^3 a(a+1)(a+2)} \ln(1 - \mathscr{A}_A), \tag{13}$$

and

$$\lambda = -\frac{3\pi}{4(a+2)\mathscr{L}_A}(1 - \mathscr{A}_A)\ln(1 - \mathscr{A}_A). \tag{14}$$

To determine the parameters of the stochastic model, we rely on a maximum likehood approach to find the parameters that minimize the least-square distance between the covariance of the simulated microstructure and the covariance that is measured on the available experimental dataset. However $\mathscr{L}_A$ is highly influenced by interconnection between particles. As many particles remains in contact due to poor interstices segmentation, computing θ only from λ and a provides a more robust algorithm.

INTERSTICES IMPLANTATION

To simulate the second scale of the microstructure, that corresponds to the interstices between the particles of the same aggregate, we rely on random Johnson-Mehl tessellations restricted to each aggregate, or connected component of the first scale of the microstructure.

Let Ω denote a given volume in $\mathbb{R}^3$. A Voronoï tessellation is a tessellation built from a Poisson point process $\mathscr{P}$ in the space $\mathbb{R}^3$. Every point x of $\mathbb{R}^3$ is associated to the class $\mathscr{C}_i$ containing all points of $\mathbb{R}^3$ closer from the point x_i of $\mathscr{P}$ than from any other point of $\mathscr{P}$. Hence, the classes $C_i, i = 1,..,N$ are defined by

$$C_i = \left\{ y \in \mathbb{R}^3, \forall j \neq i, \|x_i - y\| \leq \|x_j - y\| \right\}. \tag{15}$$

With probability one, Voronoï tessellations are normal and face-to-face. Voronoï tessellations are characterized by one single parameter, namely the intensity of the underlying point process.

The Johnson-Mehl tessellation is a sequential version of the Voronoï model [18, 20, 21, 22], where the Poisson points are implanted sequentially according to a parameter t which can conveniently be interpreted as an implantation time. All classes grow then isotropically with the same rate v, and the growth of crystal boundaries is stopped when they meet. All Poisson points falling in an existing cell are removed. From a mathematical perspective, a Johnson-Mehl tessellation is constructed from a sequential Poisson point process where the points $x_i, i = 1,..,N$ are implanted sequentially at a time $t_i, i = 1,..,N$. The classes $C_i, i = 1,..,N$ corresponding to the points $x_i, i = 1,..,N$ are defined by

$$C_i = \left\{ y \in \mathbb{R}^3, \forall j \neq i, t_i + \frac{\|x_i - y\|}{v} \leq t_j + \frac{\|x_j - y\|}{v} \right\}. \tag{16}$$

Note that when all times are set to zero, we recover the classical Poisson-Voronoï tessellation model.

In this study, to account for the interstices between grains of the same aggregate, we rely on a modified version of the Johnson-Mehl tessellation For each grain n, we simulate a random number ζ_n according to an exponential law with some mean k. The classes are now defined, for a given aggregate $\mathscr{A}$, by

$$C_i = \left\{ y \in \mathscr{A}, \forall j \neq i, t_i + \frac{\|x_i - y\|}{v} + \zeta_i \leq t_j + \frac{\|x_j - y\|}{v} \right\}, \tag{17}$$

where $\|\|$ is the geodesic distance on the set $\mathscr{B}$ defined by the first scale of the model. With this definition, we note that some points of the aggregates don't belong to any class of the Johnson-Mehl tessellation. We consider that these points form the interstices between the grains of the microstructure.

The main challenge faced using Johnson-Mehl tesselation was to quickly calculate the position of the interstices. To do so we rely on the fast marching method in 2D or in 3D [26]. This method solves boundary value problems of the eikonal equation in the spatial domain Ω:

$$\begin{aligned} |\nabla u(x)| &= \frac{1}{f(x)} \text{ for } x \in \Omega \\ u(x) &= 0 \text{ for } x \in \partial\Omega \end{aligned} \tag{18}$$

in which $u(x)$ is the arrival time of the front and $f(x)$ its propagation time. This method allows to quickly compute propagation time of closed curves from nuclei in space.

A question remains, which is how to select the initial nuclei of the tessellation and the nucleation times. While selecting the nuclei, our aim is to preserve the geometrical shape of the grains of the microstructure. The goal is to set the nuclei in the center of connected components to simulate a granulary microstructure. Therefore, we rely on the h-maxima of the distance function to generate the nuclei. The h-maxima of the distance function form connected components. For each component, we select its barycentre to be the location of a nucleus. The threshold for the h-maxima is selected after an optimization procedure that aims at minimizing the distance between the granulometries. In addition, we only keep a proportion p of the h-maxima, p being an additional parameter of the model. For each nucleus n, we denote by d_n the value of the distance function at the location of the nucleus. The nucleation time associated to nucleus n is defined to be

$$t_n = \max_m d_m - d_n. \tag{19}$$

MAXIMUM LIKEHOOD FOR PARAMETERS ESTIMATION

The parameters estimation follows a two-step process. For estimating the parameters a and λ of the first scale of the model, we compute a slice of a 3D microstructure resulting from the Boolean model. We use 1000x1000 pixels slices, taken from a larger volume to account for border effects. The spheres are implanted within this given volume, requiring it to be large enough to reach a representative copper fraction. We measure then the covariance associated to the slices. The covariance is compared with the experimental one. We aim at minimizing the least square distance between both covariances. To do so, we rely on a Nelder-Mead procedure optimizing on the parameters of the radii distribution: a and λ. Each guess of these parameters gives a value for θ according to relation (13). With good initial values, it takes less than 40 iterations to fit the experimental covariance.

For the second scale of the model, we rely on a similar procedure, this time involving the granulometry measurements, to estimate the threshold value h of the h-maxima distance that is used to select the nuclei locations, the proportion p of h-maxima that needs to be removed and the parameter of the exponential law describing interstice thickness.

NUMERICAL IMPLEMENTATION OF THE MODEL

In this section, we briefly recall the main steps of the developed algorithm and we describe the numerical implementation of the two-scale model. This implementation aims at simulating 3D microstructures while reducing calculation time. The algorithm proceeds as follows:

1. The first step of the algorithm is to simulate a Boolean model of spheres with intensity θ. The radii of the implanted spheres follow the Gamma law (4). The boolean model of spheres is simulated using the 3D vectorial VTK-based library vtkSim [10, 12]. To accelerate volume building from simulation, building was performed using subvolumes. This method allows to simulate $500 \times 500 \times 500$ voxels microstructures in 400 s (proc time) on a PC (Ubuntu 6.14 i7 2.20 GHz 6 GB RAM). The complexity of the algorithm is $O(N^2)$ with N the number of voxels in the volume.
2. The second step of the algorithm is the simulation of the interstices. The algorithm follows the following steps.
   (a) Calculation of the distance function for the microstructure obtained from the Boolean model of spheres
   (b) Determination of the h-maxima of the distance function for a specified h. When the h-maxima form a connected component, the algorithm extracts its barycenter.
   (c) Random selection of nuclei from the barycenters. The algorithm selects a given barycenter with a specified probability p. Each nucleus is then given a nucleation time according to relation (19).
   (d) The propagation time of each nucleus is computed using the fast marching method

through the Python extension module scikit-fmm [1]. The algorithm complexity of the fast marching method is $O(N \ln N)$. The module takes as input the coordinates of the nuclei and a velocity map to compute the distance function. The velocity is equal to one at the locations included in the Boolean spheres and zero otherwise.

(e) The simulated microstructure is obtained from the propagation times according to relation (17).

RESULTS AND DISCUSSION

INTERSTICES SEGMENTATION

Due to large physical difference between PEEK and copper, the solutions for imaging the microstructure are very restricted. In fact optical microscopic analysis remains the best way to obtain images of satisfactory quality. For instance, scanning Electron Microscope would induce white artefacts and blur around the copper particles. In addition, in our problem, the relatively low resolution of the images makes the selection and the segmentation of the individual particles a rather difficult task. In particular, it is quite difficult to achieve a good segmentation of the PEEK interstices because of the low image resolution and poor grey gradient at the interfaces, so that some of them remain partially replaced by copper. One can see on Fig. 6 that the watershed process achieves particles separation but is not able to include each PEEK layer between them. Once segmented, separated particles in the center of Fig. 6a and Fig. 6b do feature an interstice on Fig. 6d and do not on Fig. 6c, because particles are closer. This phenomenon could be avoided with larger magnification. However it would signify larger images to keep the surface representative, hence more memory and longer processes. One must therefore keep in mind that these phenomenon induces biased assessment of morphological parameters. First, the computation of the perimeter of the copper phase, which remains highly sensitive to interstices presence, must be used carefully. This is mostly the reason which explains why we did not rely on Eq. (14) for the parameter identification phase. Second, the measurements slightly underestimate the contribution of the thinnest interstices to the thickness distribution displayed in Fig. 10.

MODEL

To estimate the adequation between the model and the experimental images, we considered several morphological criteria, namely the covariance, the granulometry and the thickness distribution of the interstices. The joint use of the covariance and the granulometry is relatively common in morphological models [15]. The granulometry provides a characterization for the size distribution of the objects that are present in the microstructure, while the covariance provides a second order statistics which characterize the scales present in the microstructure as well as their superimposition. The distribution of interstices is more specific to our model. It is a key parameter of the model: since the conductivity contrast is high between the copper particles and the polymer matrix, large interstices lead to a significant decrease of the electric conductivity of the microstructure at the macroscopic scale.

We show in Fig. 11 a slice of the simulated microstructure obtained with the parameters estimated with the maximum likehood approach. The parameters are reported in Table 1, with A_a the measured surface fraction of copper on segmented images, θ the intensity of the poisson point process, λ and a the parameters of the Gamma distribution of the spheres radii, h the h-maxima of the distance function used for selecting the nuclei of the tesselation and p the proportion of h-maxima that are randomly selected. The covariance and the granulometry of the simulated and of the experimental microstructures are shown in Fig. 12. A comparison between the thickness distribution of the interstices is displayed in Fig. 13.

Covariances and granulometries taken from simulated and segmented images shows good agreement, assessing the validity of the model. We can observe a small discrepancy, around 0.01, between the experimental and the simulated covariances for distances ranging from 10 µm to 40 40 µm. We attribute this discrepancy to the existence of a few large zones in the polymer that do not contain copper particles. These large zones can be observed in Fig. 11). To accurately simulate these empty areas, a potential solution is to introduce an additional Boolean model aimed at defining so-called exclusion zones in the microstructure. However, this requires defining additional parameters for describing the model. These parameters are difficult to estimate from the available data: since these empty zones are rarely observed, the experimental data does not provide us with a statistically relevant description of these microstructure areas. In addition, due to their scarcity, these zones have little influence on the electric conductivity of the microstructure at the macroscopic scale. Hence, since the covariance curves remain relatively close, we discarded the existence of these empty zones in our model.

A_a	θ	λ	a	k	h	p
63%	$4.8 \times 10^{-3}\,\mu m^{-3}$	2.3 µm	0.8	1.2 µm	7.26 µm	0.5

Table 1: Model parameters

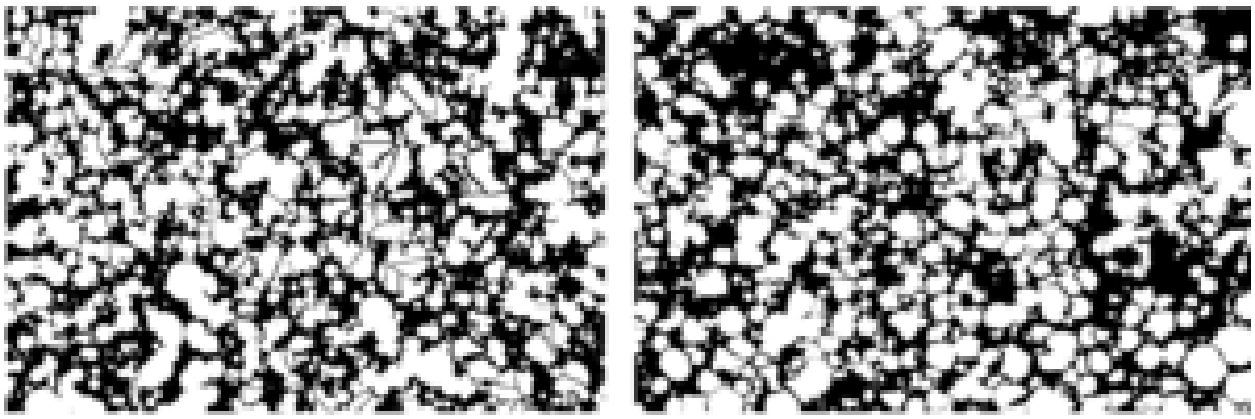

Fig. 11: Simulated microstructure after parameters optimization (left) and experimental microstructure (right), with resolution 0.484 µm

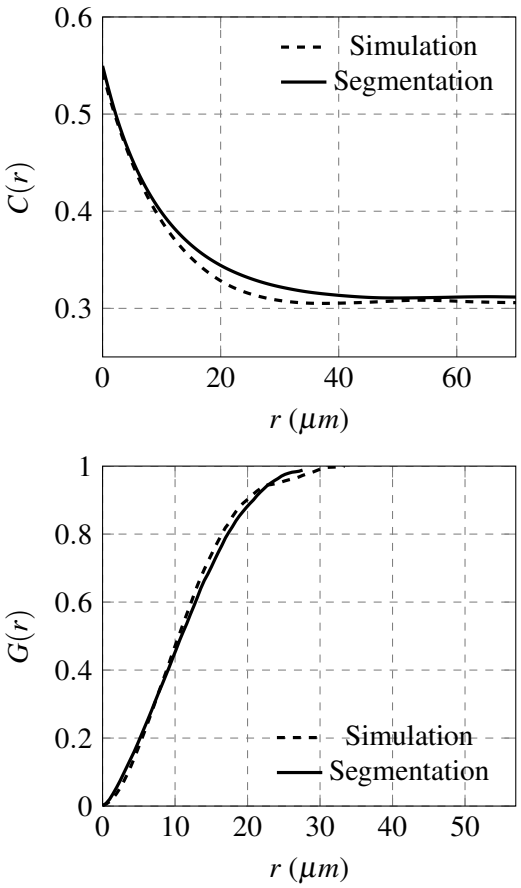

Fig. 12: Simulated and experimental microstructures comparisons between covariances (a) and granulometries (b)

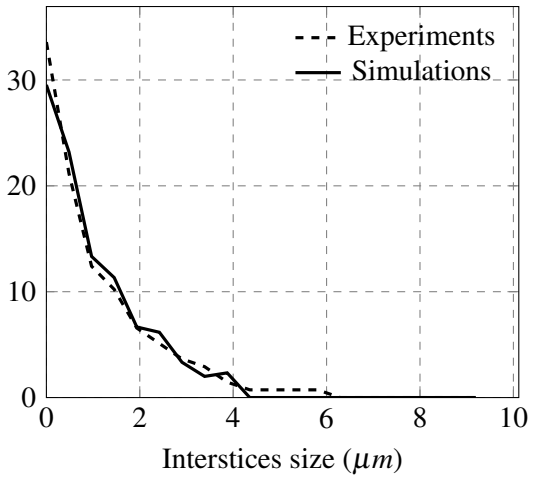

Fig. 13: Comparison between the interstice thickness distribution, as estimated on the simulated and on the experimental images.

CONCLUSION

In this article, we developed an original method to model the microstructure of a cold spray coating. The two-scale microstructure is modeled by Boolean spheres separated from each other by interstices implanted using a Johnson-Mehl tesselation. The covariance and the granulometry measured on slices of simulated microstructure fit well those from segmented images. The parameters of the model are optimized by fitting distribution law on experimental data and with a Nelder-Mead optimization algorithm.

The model allows us to simulate representative volumes of the microstructure. We assessed the representativeness of the model with the covariance, granulometry and also the distribution of interstice size.

The robust and simple segmentation process allow us to use a large amount of images without any complex preparation. The model is flexible enough to easily simulate various shape of particles or volume fraction. Three-dimensional simulation require an fast computation time to generate a small number of representative volumes of coating. These simulated microstructures will eventually allow us to investigate the physical properties of the coating without having to spray a large amount of various coating. This will be done by simulations using finite element method or Fast Fourier Transform.

REFERENCES

[1](2015). scikit-fmm. https://pythonhosted.org/scikit-fmm/.

[2]Amsellem O, Madi K, Borit F, Jeulin D, Guipont V, Jeandin M, Boller E, Pauchet F (2008). Two-dimensional (2d) and three-dimensional (3d) analyses of plasma-sprayed alumina microstructures for finite-element simulation of young's modulus. Journal of Materials Science 43:4091–8.

[3]Beauvais S, Guipont V, Jeandin M, Jeulin D, Robisson A, Saenger R (2008). Study of the porosity in plasma-sprayed alumina through an innovative three-dimensional simulation of the coating buildup. Metallurgical and Materials Transactions A 39:2711–24.

[4]Beucher S, Lantuéjoul C (1979). Use of watersheds in contour detection. In: International workshop on image processing, real-time edge and motion detection.

[5]Bobzin K, Kopp N, Warda T, Öte M (2012). Determination of the effective properties of thermal spray coatings using 2d and 3d models. Journal of thermal spray technology 21:1269–77.

[6]Chiu SN, Stoyan D, Kendall WS, Mecke J (2013). Stochastic geometry and its applications. John Wiley & Sons.

[7]Cochelin E, Borit F, Frot G, Jeandin M, Decker L, Jeulin D, Al Taweel B, Michaud V, Noel P (1999). Oxidation and particle deposition modeling in plasma spraying of ti-6al-4v/sic fiber composites. Journal of thermal spray technology 8:117–24.

[8]Delloro F, Faessel M, Proudhon H, Jeulin D, Jeandin M, Meillot E, Bianchi L (2014). A morphological approach to the modeling of the cold spray process. In: ITSC 2014. DVS.

[9]El Moumen A, Imad A, Kanit T, Hilali E, El Minor H (2014). A multiscale approach and microstructure design of the elastic composite behavior reinforced with natural particles. Composites Part B Engineering 66:247–54.

[10]Faessel M (2016). vtksim software. http://cmm.ensmp.fr/~faessel/vtkSim/demo/.

[11]Faessel M, Bilodeau M (2014). Smil simple morphological image library. In: Séminaire Performance et Généricité, LRDE.

[12]Faessel M, Jeulin D (2011). 3d multiscale vectorial simulations of random models. Proceedings of ICS13 :19–22.

[13]Figliuzzi B, Jeulin D, Faessel M, Willot F, Koishi M, Kowatari N (2016). Modelling the microstructure and the viscoelastic behaviour of carbon black filled rubber materials from 3d simulations. Technische Mechanik 32:22–46.

[14]Gasnier JB, Willot F, Trumel H, Figliuzzi B, Jeulin D, Biessy M (2015). A fourier-based numerical homogenization tool for an explosive material. Materiaux Techniques 103:308.

[15]Jean A, Jeulin D, Forest S, Cantournet S, N'guyen F (2011). A multiscale microstructure model of carbon black distribution in rubber. Journal of microscopy 241:243–60.

[16]Jeandin M, Borit F, Guipont V, Decker L, Jeulin D, Suzuki M, Sodeoka S (1999). Lattice gas modelling in thermal spraying. Surface engineering 15:191–4.

[17]Jeulin D (2012). Morphology and effective properties of multi-scale random sets: A review. Comptes Rendus Mecanique 340:219–29.

[18]Johnson WA, Mehl RF (1939). Reaction kinetics in processes of nucleation and growth. Trans Aime 135:396–415.

[19]Miles RE (1972). The random division of space. Advances in applied probability :243–66.

[20]Møller J (1989). Random tessellations in $\mathbb{R}^d$. Advances in Applied Probability :37–73.

[21]Møller J (1992). Random johnson-mehl tessellations. Advances in applied probability :814–44.

[22]Møller J (1994). Lectures on random Voronoi tessellations. Springer.

[23]Otsu N (1975). A threshold selection method from gray-level histograms. Automatica 11:23–7.

[24]Schneider R, Weil W (2008). Stochastic and

integral geometry. Springer Science & Business Media.

[25]Serra J (1982). Image analysis and mathematical morphology. Academic press.

[26]Sethian JA (1996). A fast marching level set method for monotonically advancing fronts. Proceedings of the National Academy of Sciences 93:1591–5.

[27]Soille P (2003). Morphological image analysis: principles and applications. Springer-Verlag New York, Inc.

[28]Torquato S (2002). Random heterogeneous materials: microstructure and macroscopic properties, vol. 16. Springer.

[29]Vincent L, Soille P (1991). Watersheds in digital spaces: an efficient algorithm based on immersion simulations. IEEE Transactions on Pattern Analysis Machine Intelligence :583–98.

[30]Zeng QH, Yu AB, Lu GQ (2008). Multiscale modeling and simulation of polymer nanocomposites. Progress in Polymer Science 33:191–269.

Cold spray of metal-polymer composite coatings onto Carbon Fiber-Reinforced Polymer (CFRP)

V. Bortolussi, F. Borit, A. Chesnaud, M. Jeandin, Evry /F, M. Faessel, B. Figliuzzi, F. Willot, Fontainebleau /F, K. Roche, G. Surdon, Argenteuil /F

The growing use of Polymer-Matrix Composite (PMC) materials within transport industry raises new security concerns, especially those due to lightning. To protect these electrically insulating materials, conductive coatings can be applied. Due to the high level of required properties, cold spray is believed to be an effective way to achieve these coatings. Recent studies showed that obstacles remained to be overcome when cold spraying metallic particles onto Carbon Fiber-Reinforced Polymer (CFRP). These are rather due to a poor adhesion of metallic particles onto carbon fibers, which prevents coating build-up. This study therefore developed the use of PEEK addition to metallic powder. The goal is to promote the coating-substrate bond strength provided that the coating could be conductive. The work focusses on composite coatings made of PEEK thermoplastic polymer powder and copper powder. The influence of spraying parameters, powder shape, size and distribution were investigated for various polymer ratios. Depending on these parameters, various microstructures could be achieved, which resulted in different electrical and bonding properties. Coating cross-sections were studied using morphological operations coupled with quantitative image analysis. Relevant parameters to feed a model for simulation of the sprayed microstructure were thus determined. This model as an effective optimization tool allowed to carefully select powders and mixture composition to produce adherent and electrically conducting coatings. Electrical properties were assessed using the Van der Pauw method with dedicated device and samples. The latter were specifically designed to lead to significant and accurate resistance measurements. These measurements showed the feasibility of PEEK-copper composite coating of CFRP. Incidentally, beyond electrical applications, this type of cold-sprayed composites can be claimed to be suitable for a large range of applications.

1 Introduction

The manufacturing of most recent commercial aircrafts involves lighter materials such as Carbon Fiber-Reinforced Polymer (CFRP). These materials often combine stacks of carbon fibers embedded in a matrix made of a thermoplastic polymer such as PEEK (Poly-Ether-Ether-Ketone). Unlike aluminum alloys, CFRP shows a high electrical resistivity due to the polymer matrix which is not suitable for protection against lightning impact. To promote this protection, aircraft manufacturers use lightning screens, which involve complex manufacturing processes. Amongst thermal spray processes, cold spray is believed to be an elegant solution to coat CFRP with electrically-conductive materials. The past 2 years showed an increasing number of articles dealing with metallic cold spray coating onto polymers and composite materials. In 2006, Sturgeon et al. [1] investigated for the first time cold spray coating of carbon fiber/PEEK with aluminum. They achieved adherent and dense coating using helium as a spraying gas and observed the behavior of the coating under thermal cycling. However, it must be mentioned that the PEEK matrix was reinforced with short carbon fibers, which means a microstructure significantly different from that with continuous fibers. Short fibers globally and locally reinforced PEEK on which the coating was sprayed. A similar study was presented by Zhou et al. [2] in 2011, still using short carbon fibers/PEEK composite on which they could spray aluminum and copper. However, to be deposited successfully, copper had to be sprayed onto an aluminum bond coat. A more recent study focused on epoxy matrix composite which exhibited a different thermomechanical behavior in the cold spray process. Affi et al. [3] stated the difficulty to grow an aluminum coating onto epoxy. They used a plasma-sprayed aluminum underlayer on which the cold spray coating could grow. They also investigated the effect of the granulometry of the aluminum powder. In 2014, Che and Yue [4] used the cold spray to coat a continuous carbon fiber/epoxy composite with aluminum, copper and tin. Only scarce particles of tin were reported to be adherent to the substrate, whereas they could not obtain a coating with copper and aluminum. These papers showed the difficulty to achieve dense and adherent coatings onto both carbon fibers and epoxy [5]. It appears that thermoset polymers are hardly suitable for cold spray while metallic coating can be obtained onto thermoplastic polymers. Hence some authors only focused on non-reinforced polymer substrates, with good results [5-7].

This paper focuses on the coating of continuous carbon fibers/PEEK composites with copper using cold spray. Previous studies showed that copper particles rebound on carbon fibers and break them at the impact. In this work to limit fiber failure and obtain an adherent coating, a method was proposed i.e. spraying a mixture of PEEK powder with copper powder. This method can be claimed to be original. One must refer only to a somewhat similar experiment focused on spraying various ratios of polymer powder with copper and aluminum in order to obtain frictionless but electrically conductive coatings [8].
In the present paper, the influence of cold spray parameters was investigated as well as powder granulometry and particle shape. The concept of critical velocity was not valid in this specific case. Then the coating microstructure was observed and analyzed. A

morphological model of the coating was then developed from quantitative image analysis of the same microstructure.
Morphological models are very useful to determine numerically physical and mechanical properties of multiphased materials exhibiting periodic or random structures. They allow to perform numerous numerical simulations on representative volumes. Varying the spatial distribution and size parameters of the phases can thus be easily done to investigate their influence on materials properties, primarily those of coatings [9-13]. In this study, the model would be used to numerically perform a morphological optimization of the microstructure, allowing to select the best powder to lead to optimized properties.

2 Materials and Processing

Two copper powders were sprayed: the first powder was a high-purity (≥99.95 wt%) spherical copper powder. Particles size ranged from 10.6 µm (d_{10}), to 33.1 µm (d_{90}) with a d_{50} of 19.6 µm as obtained by laser granulometry. The second powder was an irregular and coarser copper powder, the particle size of which ranged from 11.4 µm (d_{10}), to 114 µm (d_{90}) with a d_{50} of 57.6 µm. Copper powders were mixed with Vicote 702 PEEK powder, the particle size of which ranged from 26.5 µm (d_{10}), to 88.5 µm (d_{90}) with a d_{50} of 52.8 µm. The mixture of PEEK and copper was observed with a SEM. Spherical copper particles appeared in bright grey whereas irregular PEEK particles appeared darker, **Fig. 1.**

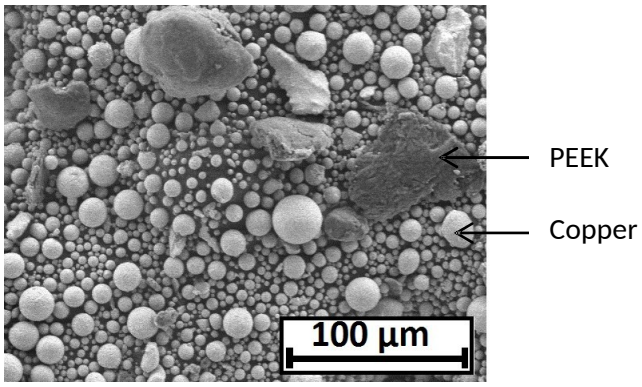

Fig. 1. SEM view of the powder mixture

This paper focuses on only one mixture of powder i.e. 80 vol.% of copper and 20 vol.% of PEEK, termed as 80/20, **Fig.1.** However, tests were performed using various ratios. The substrates were small samples of 25x25x2 mm^3 made of aeronautical grade continuous carbon fibers plies embedded in a PEEK matrix. Plain Victrex PEEK 450G samples of the same dimensions were also coated. PEEK in the composite, Victrex 450G and powdered PEEK, were all three different. However, a common glass transition of 140 °C and a melting temperature of 330 °C were considered. The CFRP surface presented an original rugosity with small bump of PEEK and valley with carbon fibers at the bottom.

Spraying experiments were carried out using a KINETICS 3000M cold spray system by CGT-Gmbh with a “MOC” nozzle perpendicular to the substrate. Spraying pressure and temperature were optimized as well as the powder flow rate, passing speed and passing step. Stand-off distance was kept at 80 mm from the substrate and all samples were sprayed in one pass only.
Coatings were cross-sectioned, polished, and metallized using a Cressington sputter coater to be observed with a Leica optical microscope. Metallization greatly enhanced the contrast between the various phases in the microstructure, which improved image analysis. Analyses were performed using ImageJ and mostly SMIL [14] in python scripts.
The electrical resistance of the coatings was checked with a simple digital ohmmeter. Coating samples for electrical conduction measurements were sprayed onto thinner (<1 mm) substrates of PEEK for their electrical behavior being investigated using the Van der Pauw method [15]. Contrary to CFRP, PEEK is insulating, which thus allowed to measure the conductivity of the coating only. These coatings were sprayed through a mask to obtain a cloverleaf shape with a diameter of 20 mm. This shape is optimal for the Van der Pauw method because it concentrates current lines in the middle of the samples, thus reducing measurement errors. The resistance of the coating were therefore measured in the various current ranges of 1 mA, 10 mA, 100 mA, 500 mA and 1 A in a HFS600E-PB4 Linkam system chamber with a Keithley 2450 Sourcemeter.

3 Results

Coatings were first optimized based on visual inspection of surface coating homogeneity and their surface mass. The first goal was to identify spraying parameters for the best coating build-up onto the substrate. Investigations were made on process gas parameters i.e. pressure and temperature. The particle surface flow rate seen by the substrate which depends on the passing speed, the passing step and the powder flow rate was also investigated.

3.1 Pressure and temperature influence

The influence of temperature and pressure of the carrier gas on coating build-up was investigated. All sprayings were performed with the same particle surface flow rate (i.e. using given passing step, speed and powder flow rate). Pressure and temperature ranged from 300 to 500 °C and 1.0 to 2.0 MPa, respectively. Coatings made of spherical copper particles tended to grow easily compared to those made of irregular particles. In the case of spherical copper particles, the optimized parameters seemed to be 1.5 MPa and 400 °C. In the case of irregular particle, thickest coatings were obtained at 1.5 MPa and 500 °C. However, these graphs do not show the coating homogeneity, **Fig. 2.** Under certain conditions, the coatings exhibited a high surface mass with many large

defects at the surface such as craters or uncoated zones.

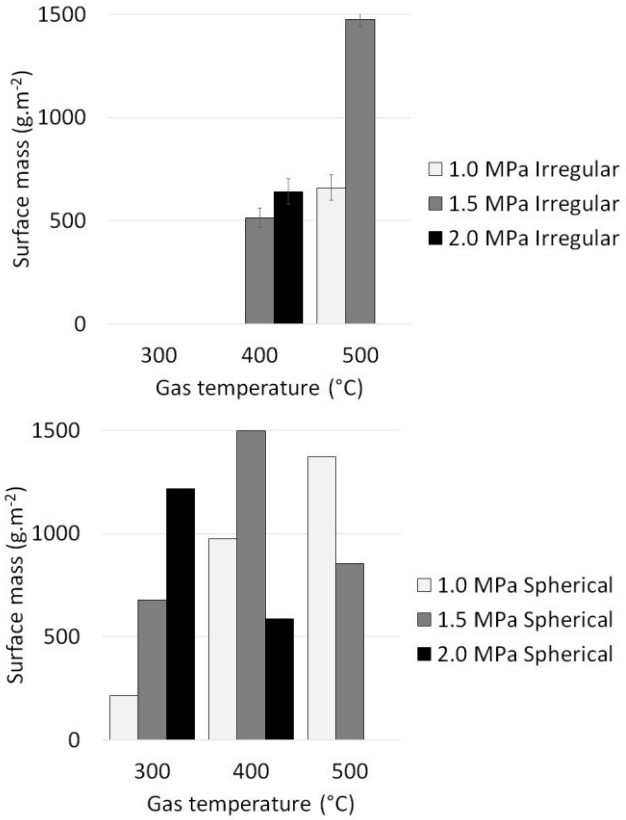

Fig. 2. Influence of the gas parameters on the surface mass of the coatings

3.2 Influence of particle surface flow rate

The influence of the particle surface flow rate was investigated with gas parameters kept at 1.5 MPa and 400 °C. The passing speed and step ranged from 100 to 300 mm.s $^{-1}$ and from 1 to 3 mm respectively. First, homogeneous coatings could be sprayed with a lower speed and a smaller step with non-optimal gas parameters, as shown on sample (a), **Fig. 3.**

(a) Spherical copper particles	(b) Spherical copper particles	(c) Irregular copper particles
1.5 MPa, 300 °C, passing speed: 100 mm.s^{-1}	1.5 MPa, 400 °C, passing speed: 300 mm.s^{-1}	1.5 MPa, 400 °C, passing speed: 100 mm.s^{-1}

Fig. 3. Top views of coatings at different spraying parameters

Second, when using spherical copper particles, increasing the passing speed by 100 mm.s^{-1} or the passing step by 1mm had exactly the same influence on the deposited mass. However, coating topography changed. Third, still with spherical particles, the particle surface flow rate and the gas parameters had an equal influence on coating build-up. It was possible to achieve thick and homogeneous coating by optimizing the temperature and pressure or the passing speed, step or flow rate. For irregular copper particles, the spraying window was narrower. Particle surface flow rate should be high enough to avoid surface defects but it led to thick coatings, i.e. with a high surface mass.

3.3 Coating microstructure

The microstructure of the coating showed two different phases. The PEEK powder was highly deformed, to result in a grey matrix which was surrounded by bright yellow copper particles. A third “phase” made of black holes was due to debonded copper particles. Spherical copper particles exhibited plastic deformation solely when impacting each other. They therefore mostly remained spherical, except on their impacted side.

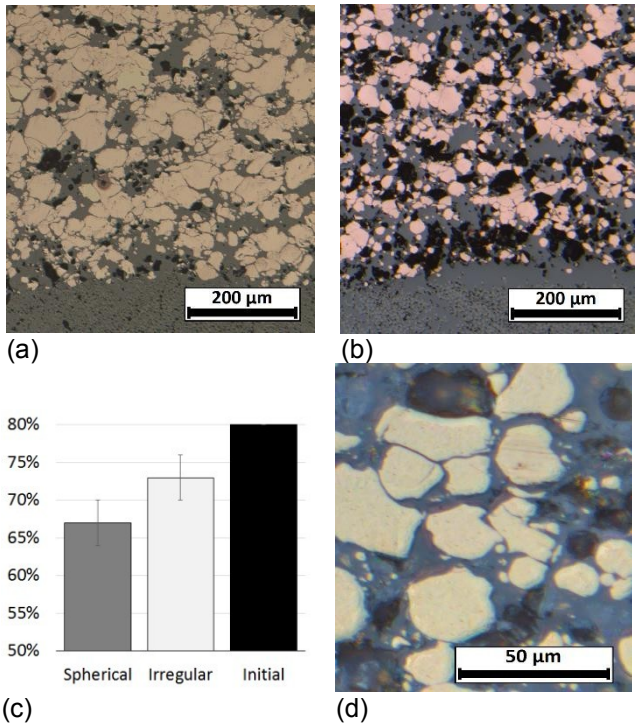

Fig. 4. Microstructure with (a) irregular particles, (b) spherical particles, (c) copper volume ratios in the coatings, (d) magnified view of (b)

Cross-section images were used for quantitative phase analysis. The surface fraction and density of copper along the vertical axis were investigated. In microstructures which involved spherical copper, the volume ratio of copper could be approximated by the surface ratio when averaged over a large number of images. The averages were computed with an automatic image segmentation method from 13 images of 2560x1920 pixels² with a resolution of 0.242 µm per pixel. The coatings made of irregular particles showed 73 vol.% of copper (a), and those made of spherical copper particles 67 vol. %, **Fig. 4** (b).
Powder shape could be responsible for the difference in copper ratio between the spherical and irregular particles. These measurements also showed that approximately 10 vol.% of copper were missing in the

coating. These particles might have rebounded due to a lower velocity when impacting other copper particles. At a higher magnification, one could see that copper particles were well packed but often separated by a thin gray gap. It was believed that this gap was made of highly-deformed PEEK which surrounded the particles i.e. PEEK filled gap. This led to a microstructure which was slightly different from purely metallic coatings obtained by cold spray. PEEK prevented direct contact, diffusion and chemical bonding. Moreover, many deformed particles were still separated by PEEK even on the impacted side. The number of contacts between irregular particles was higher than that when using spherical particles.

3.4 Morphological model

The presence of PEEK filled gaps and the morphology of the microstructures could be assumed to govern the electrical conductivity of the coating. To simulate the current paths, a 3D morphological model was developed. The goal was to be able to investigate into the electrical behavior, from optimization of the metal phase morphology, and later from the selection of the best powder shape and size. The development of such model involved 3 steps:

- Segmentation of cross-sectional images to separate phases and remove visual artifacts or defects.
- Image analysis to extract image quantitative information according to 3 morphological criteria, termed correlation functions.
- Multi-scale morphological model development and optimization based on the 3 previously-mentioned morphological criteria extracted from experimental images.

The segmentation process resulted in two images: a binary image with copper particles in white and PEEK matrix in black, **Fig. 5.** (d). Debonded particles were added numerically to fill the holes. The second image showed labeled particles which allowed us to assess the efficiency of the process to segment neighboring particles, **Fig. 5.** (c). The main drawback in the segmentation process was that it could not segment every PEEK filled gap which separated close particles. The resolution and the color gradient were not good enough, so when the particles were too close, the process filled the gap with copper.

In the binary images three morphological criteria were considered to characterize the microstructure. The first criterion was the covariance, the probability that for a given point in the copper phase, if it was translated from a vector, it was still in the copper phase. This criterion corresponded to the spatial distribution of the copper numerically. The second criterion was the cumulative granulometry obtained by opening. This criterion described the size of copper phase. The third criterion related to the distribution of PEEK filled gap size. This criterion was approximate as the algorithm could not segment all the PEEK filled gap. This distribution appeared to follow a modified exponential distribution of parameters k.

Microstructures modeling involved two scales. The first scale was that of the copper particles. These were described by a Boolean model of spheres. The diameter of each sphere followed a gamma distribution of parameters a and λ. Boolean spheres were distributed spatially according to θ, the intensity of the Poisson's point process. Hence, the first scale involved three parameters which were calculated from the granulometry and the covariance through experimental images. Boolean spheres were distributed using an initial set of parameters in a 512x512xλ voxels space. The covariance and the granulometry were computed on a slice of this simulated microstructure. θ, a and λ were optimized using a "Nelder-Mead" algorithm to fit the experimental covariance and granulometry. The "Nelder-Mead" algorithm involved a simplex method, robust and useful in this case as there was no direct mathematical link between covariance, granulometry and these parameters. Moreover, to simplify the optimization process, a constitutive equation was derived from stereological formula linking θ, a, λ and the experimental surface ratio of copper.

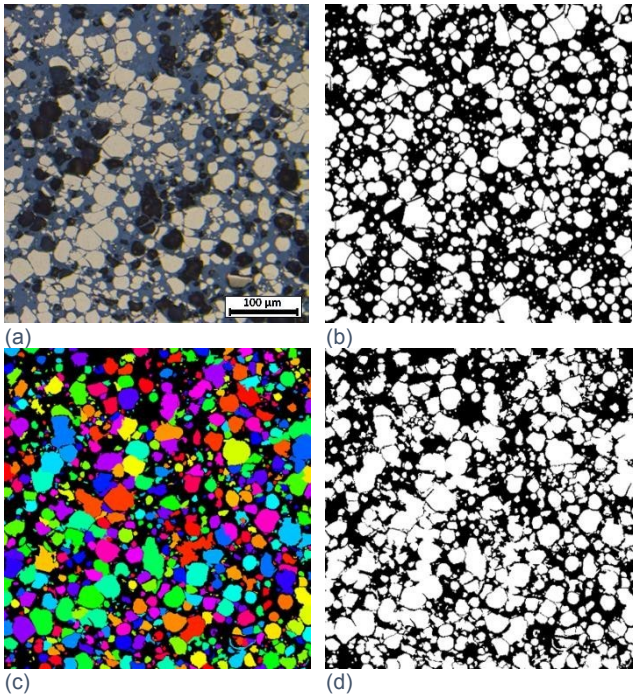

Fig. 5. (a) Original microstructure, (b) simulated microstructure, (c), (d) segmented microstructure

The second scale was that of the PEEK filled gap between neighboring particles. In the first scale, aggregates of particles were modeled by intersecting spheres, so most of them needed to be separated as in the real microstructure. In every aggregate of particles (connex spheres), germs were implanted in the center of the particles. On each germ a cell grew following a "Johnson-Mehl" tessellation. The cell nucleation and growth were time dependent. Cell boundaries were considered as PEEK filled gaps and were colored in black. They could therefore separate the particles from each other. The thickness of the boundaries was randomly computed following the exponential

distribution which fitted the PEEK filled gap size distribution. Hence a simulated microstructure could be computed according to the three morphological criteria, which met the experimental microstructure, **Fig. 5** (b).

3.5 Electrical behavior of the coating

Resistance measurements showed that coatings made of spherical copper hardly conducted electricity. In contrast, when using the irregular shaped copper, one could measure a resistance which felt down to below 1 Ω, using a mere portable ohmmeter. However, the conductivity of these coatings needed to be investigated thoroughly using an insulating substrate. Coatings sprayed onto PEEK substrate were first cross-sectioned to check whether the microstructure and the copper ratio were identical to those sprayed onto CFRP. Copper ratios were measured using the previously-described segmentation method. The difference was small enough to ascertain the microstructures were similar, **Fig. 6.**

Substrate	Final average surface ratio of irregular copper	Standard deviation
CFRP	73%	3%
PEEK	68%	4%

Fig. 6. Copper ratio in coatings onto two substrates

Two thicknesses for the 80/20 coating were sprayed. Increasing the passing speed from 100 to 200 mm.s $^{-1}$ decreased the mean thickness from 781 µm to 358 µm. Decreasing thickness also increased the number of surface defects, which consequently reduced the conductivity. The conductivity was determined from four measurements, along each side of the cloverleaf-like sample. Some slight anisotropy was showed from vertical and horizontal measurements, which might be due to defects, incorrect probe positioning or sample dissymmetry. When increasing the current intensity, a slight resistance drop was observed. Finally, regardless of thickness, under a 1 A current there was a quick damage of the coating which could burn and corrode. This left current line marks at the surface. Intensity was high enough to burn PEEK and heat up the whole sample.

Conductivity appeared to depend on coating thickness with a drop of 1500 S.m $^{-1}$ when passing from 781 µm to 358 µm. This behavior was questionable but one can assume that the thicker the coating was, the more complex it was. This involved the paths between copper particles from one side to the other, which led to an electrical loss. At 1 A, the coating quickly burnt, which decreased the measured resistance. The presented value was not therefore obtained in an equilibrium state.

Conductivities could be compared with that obtained on similar samples of pure cold spray copper onto PEEK. The conductivity of the composite coatings was shown to be three decades below the conductivity of pure copper coatings, which, incidentally could reach the bulk copper conductivity i.e. 6.e7 S.m $^{-1}$, **Fig. 7.**

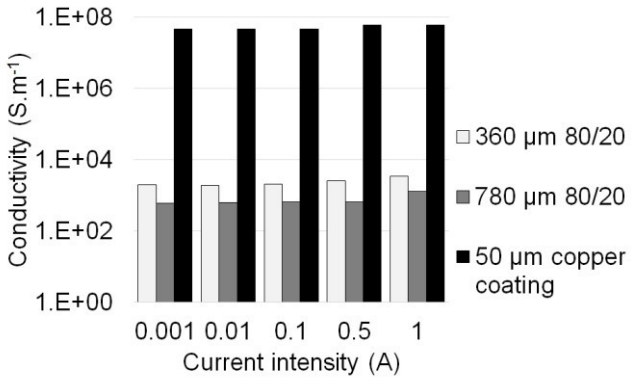

Fig. 7. Coatings conductivity

4 Discussion

4.1 Coating build-up

First, while investigating the influence of cold spray parameters, the goal was also to control the thickness and the homogeneity of the coating to obtain low-thickness, homogeneous and conductive coatings. The influence of gas pressure and temperature was studied. The optimum spraying window was shown to involve a low pressure with a rather high temperature. Moreover, the particle surface flow rate was seen to have a similar or higher influence on coating build-up when compared to that of gas parameters. A typical spraying pressure for pure copper is 2.0 MPa. One may therefore assume that the critical velocity of copper does not govern the build-up and homogeneity of the coating. These are mainly due to the presence of PEEK. This leaves bonding between deformed copper particles as a second order mechanism. This is also confirmed by the fact that the lower the pressure and the higher the temperature were, the thicker the coating was.

Second, coating build-up highly depends on the particles surface flow which is a combination of the passing speed, passing step width and powder flow rate. For example, when spraying irregular powder changing the passing step by 1mm or the passing speed by 100 mm.s^{-1} led to a similar surface mass evolution. On the other hand, this result was not valid for the spherical powder. A thorough study was carried out to compare the behavior of the two copper powders, leading to a qualitative model of the composite coating build-up. The build-up exhibits a similar non-linear behavior between the two copper powders. This behavior was particularly exhibited when reducing the particle surface flow rate with the two powders to result in a low-thickness (as low as possible but homogeneous) coating. With the spherical powder, a 100 µm thick and homogeneous coating could be achieved, which however remained insulating. Cross-section observations showed that the coatings contained in fact only scarce copper particles. With the irregular copper, reducing the particle surface flow rate

led to some large heterogeneity with many surface defects. This could be explained by the size of the particles.
Coating build-up is believed to be a two-stage process, which depends on the type of particle (fine spherical or coarse irregular), **Fig. 8.**

- Fine copper particles impact the substrate surface and rebound due to the absence of PEEK, coarse PEEK particles impact the surface at the same time as for copper particles. They adhere to the fibers, while copper particles are embedded in larger PEEK particles.
- Copper particles impact the previously-sprayed layer, deformed on copper or are embedded into PEEK.

- Coarse particles impact the substrate surface and rebound. They cannot be embedded into PEEK because of their size.
- Once a few amount of PEEK adheres to the surface with embedded smaller copper particles, larger particles finally impact, stacks or rebound. Their irregular shape can limit rebound and promotes anchoring in the already-deposited layers.

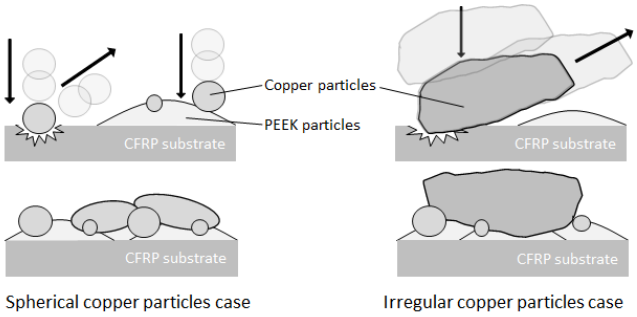

Fig. 8. Schematic illustration of the two-stage build-up process for two types of copper shape

This build-up process would explain why it was possible to obtain low-thickness coatings with spherical particles. At a lower particle surface flow rate only the first layer i.e. a sort of bond coat was sprayed. This corresponds to the first stage of the process. This layer does not contain enough copper particles to be conductive. With coarser particles sprayed at a low particle surface flow rate this type of layer cannot be obtained, since it produces a rough surface with defects. This highlights the role of the particle surface flow rate, which therefore controls PEEK deposition at the surface, allowing the coating to build-up.
The key phenomenon leading to this type of microstructure remains unknown. More precisely, the question is to know when does copper is embeded into PEEK. Is it during its flight through the nozzle or at the impact?

4.2 Electrical behavior and microstructure

The study of the microstructure led to conclude first that a significant amount of copper is lost during spraying, one may assume due to rebounds. Second, even at a high copper ratio, the metallic phase formed by the spherical particles does not percolate. The particles remain separated by thin layer of PEEK. This phenomenon seems to be unavoidable. Image analysis showed that most spherical particles were non connex, while many irregular ones were. An original morphological model was therefore developed to investigate various particle morphologies as the PEEK filled gap size distribution was approximately the same for the two types of microstructures. A higher number of contacts between irregular copper particles was assumed to govern the coating conductivity.

5 Conclusion

An original method was developed to coat Carbon Fiber-Reinforced Polymer by cold spray using polymer mixed with copper powders to result in a conductive layer. The resulting composite coatings were optimized through the study of the deposited surface mass depending on process parameters, copper particles shape and size. Interpretations of the phenomenon leading to the build-up were proposed. A morphological analysis method was developed to investigate into coating microstructures. The extraction of relevant data on the copper phase fed a morphological model of the coating microstructure. Finally, the Van der Pauw method was applied on geometrically optimized samples to assess the conductivity of the coatings. It was shown that coatings made of irregular copper particles could reach 1e3 $S.m^{-1}$ whereas those containing spherical particles remained insulating. These phenomena were mostly explained using the developed simulation tools coupled with investigation of microstructures and coating build-up.

6 Outlook

This work highlighted the interest in composite cold-sprayed coatings to achieve multi-property materials. A further goal would be to achieve gradient composite coatings in cold spray e.g. using multiple powder feeders. In this study, the polymer was shown to be an efficient coating binder. Moreover, its combination with rigid materials allowed to achieve dense coatings. Its mechanical behavior in cold spray should require to be further studies, with mechanical simulation and/or in-situ characterization during spraying.
Last but not least, morphological models can be expected to be developed as powerful tools to optimize coatings properties which depend on particle morphology. Laborious and systematic spraying campaign could thus be avoided.

7 Acknowledgments

This work was carried out within the “C.O.MET” FUI program. The authors would like to thank all the

members of the program consortium and BPI France, Pôle Astech, Pôle de la céramique, Pôle des microtechniques and DGAC for financial support. This material is based upon work supported by the Air Office of Scientific Research, Air Force Material Command, USAF under award No. FA9550-15-10461.

8 References

[1] Sturgeon, A., B. Dunn, S. Celotto, and W. O'Neill: Cold Sprayed Coatings for Polymer Composite Substrate. ESA SP, 616 (2006).

[2] Zhou, X. L., A. F. Chen, J. C. Liu, X. K. Wu, and J. S. Zhang: Preparation of metallic coatings on polymer matrix composites by cold spray. Surface and Coatings Technology 206, no. 1 (2011): 132-136.

[3] Affi, J., H. Okazaki, M. Yamada, and M. Fukumoto: Fabrication of aluminum coating onto CFRP substrate by cold spray. Materials Transactions 9, no. 52 (2011): 1759-1763.

[4] Che, H. Q., and S. Yue: Cold Spray of Carbon Fiber Reinforced Polymer for Lightning Strike Protection. International Thermal Spray Conference. Barcelona: DVS, (2014).

[5] Ganesan, A., M. Yamada, and M. Fukumoto: Cold spray coating deposition mechanism on the thermoplastic and thermosetting polymer substrates. Journal of thermal spray technology 22, no. 8 (2013): 1275-1282.

[6] Lupoi, R., and W. O'Neill: Deposition of metallic coatings on polymer surfaces using cold spray. Surface and Coatings Technology 7, no. 205 (2010): 2167-2173.

[7] Giraud, D., F. Borit, V. Guipont, M. Jeandin, and J. M. Malhaire: Metallization of a Polymer using Cold Spray: Application to Aluminum Coating of Polyamide 66. International Thermal Spray Conference. DVS, (2012).

[8] Papyrin, A., Kosarev, V., Klinkov, S., Alkhimov, A. and Fomin, V. M.: Cold spray technology, Elsevier, (2006)

[9] Jeandin, M., F. Borit, V. Guipont, L. Decker, D. Jeulin, M. Suzuki, and S. Sodeoka: Lattice gas modelling in thermal spraying. Surface engineering 15, no. 3 (1999): 191-194.

[10] Amsellem, O., K. Madi, F. Borit, D. Jeulin, V. Guipont, M. Jeandin, E. Boller, and F. Pauchet: Two-dimensional (2D) and three-dimensional (3D) analyses of plasma-sprayed alumina microstructures for finite-element simulation of Young's modulus. Journal of Materials Science 43, no. 12 (2008): 4091-4098.

[11] Beauvais, S., V. Guipont, M. Jeandin, D. Jeulin, A. Robisson, and R. Saenger: Study of the porosity in plasma-sprayed alumina through an innovative three-dimensional simulation of the coating buildup. Metallurgical and Materials Transactions A 11, no. 39 (2008): 2711-2724.

[12] Bobzin, K., N. Kopp, T. Warda, and M. Öte: Determination of the effective properties of thermal spray coatings using 2d and 3d models. Journal of thermal spray technology 6, no. 21 (2012): 1269-1277.

[13] Delloro, F., M. Faessel, H. Proudhon, D. Jeulin, M. Jeandin, E. Meillot, and L. Blanchi: A morphological approach to the modelling of the cold spray process. International Thermal Spray Conference. Barcelona: DVS, (2014): 221-226.

[14] Faessel, M., and M. Bilodeau: Smil simple morphological image library. Séminaire Performance et Généricité. LRDE, (2014).

[15] Van der Pauw, L. J.: A method of measuring specific resistivity and hall effect of discs of arbitrary shape. Philips Res. Rep. 13(1958): 1-9.

REPORT DOCUMENTATION PAGE

Form Approved
OMB No. 0704-0188

1. REPORT DATE *(DD-MM-YYYY)*	2. REPORT TYPE	3. DATES COVERED *(From - To)*
14-12-2017	Final Technical	15/09/2015 to 15/09/2017

4. TITLE AND SUBTITLE
Stochastic Models for Cold Sprayed Microstructures

5a. CONTRACT NUMBER

5b. GRANT NUMBER
FA9550-15-1-0461 DEF

5c. PROGRAM ELEMENT NUMBER

6. AUTHOR(S)
Willot, François
Bortolussi, Vincent
Jeandin, Michel
Figliuzzi, Bruno
Faessel, Matthieu

5d. PROJECT NUMBER

5e. TASK NUMBER

5f. WORK UNIT NUMBER

7. PERFORMING ORGANIZATION NAME(S) AND ADDRESS(ES)
Centre for Mathematical Morphology
Dept. of Mathematics
35 rue St Honore
77300 Fontainebleau, France

8. PERFORMING ORGANIZATION REPORT NUMBER

9. SPONSORING/MONITORING AGENCY NAME(S) AND ADDRESS(ES)
AFOSR
875 N. Randolph St.,
RM 3112
Arlington, VA 22203-1954

10. SPONSOR/MONITOR'S ACRONYM(S)

11. SPONSOR/MONITOR'S REPORT NUMBER(S)

12. DISTRIBUTION/AVAILABILITY STATEMENT
Distribution A - Approved for Public Release

13. SUPPLEMENTARY NOTES

14. ABSTRACT

We study the microstructure of cold sprayed films of copper particles deposited onto a carbon fiber reinforced polymer. The microstructure of the coating is made of a packing of seemingly round-shaped particles of varying sizes embedded in a polymer matrix. The copper particles are separated by thin interstices. The coating is designed to cover the body of recent commercial aircrafts. Its role is to protect the aircraft from lightning impact by ensuring that the surface is conductive enough to evacuate electrical charges. A high resistivity contrast is observed between the copper particles and the polymer matrix. Therefore, the global resistivity of the material is highly dependent on the microstructure geometry. Following an approach commonly used in materials science, to investigate its influence on the electrical properties of the global material at the macroscopic scale, we design a 3D multiscale stochastic model that enables us to simulate the microstructure. The model is based upon a generalization of the classical Johnson-Mehl tessellation, which accounts for the interstices that appear between copper particles. The method is very general and could potentially be applied to model any microstructure exhibiting similar interstices between aggregates of particles.

15. SUBJECT TERMS
Colspray, models of random structures, stochastic geometry, stereology

16. SECURITY CLASSIFICATION OF:			17. LIMITATION OF ABSTRACT	18. NUMBER OF PAGES	19a. NAME OF RESPONSIBLE PERSON
a. REPORT	b. ABSTRACT	c. THIS PAGE			François Willot
U	U	U	U		19b. TELEPHONE NUMBER *(Include area code)* +33 16469 4807

Reset

Standard Form 298 (Rev. 8/98)
Prescribed by ANSI Std. Z39.18
Adobe Professional 7.0

INSTRUCTIONS FOR COMPLETING SF 298

1. REPORT DATE. Full publication date, including day, month, if available. Must cite at least the year and be Year 2000 compliant, e.g. 30-06-1998; xx-06-1998; xx-xx-1998.

2. REPORT TYPE. State the type of report, such as final, technical, interim, memorandum, master's thesis, progress, quarterly, research, special, group study, etc.

3. DATES COVERED. Indicate the time during which the work was performed and the report was written, e.g., Jun 1997 - Jun 1998; 1-10 Jun 1996; May - Nov 1998; Nov 1998.

4. TITLE. Enter title and subtitle with volume number and part number, if applicable. On classified documents, enter the title classification in parentheses.

5a. CONTRACT NUMBER. Enter all contract numbers as they appear in the report, e.g. F33615-86-C-5169.

5b. GRANT NUMBER. Enter all grant numbers as they appear in the report, e.g. AFOSR-82-1234.

5c. PROGRAM ELEMENT NUMBER. Enter all program element numbers as they appear in the report, e.g. 61101A.

5d. PROJECT NUMBER. Enter all project numbers as they appear in the report, e.g. 1F665702D1257; ILIR.

5e. TASK NUMBER. Enter all task numbers as they appear in the report, e.g. 05; RF0330201; T4112.

5f. WORK UNIT NUMBER. Enter all work unit numbers as they appear in the report, e.g. 001; AFAPL30480105.

6. AUTHOR(S). Enter name(s) of person(s) responsible for writing the report, performing the research, or credited with the content of the report. The form of entry is the last name, first name, middle initial, and additional qualifiers separated by commas, e.g. Smith, Richard, J, Jr.

7. PERFORMING ORGANIZATION NAME(S) AND ADDRESS(ES). Self-explanatory.

8. PERFORMING ORGANIZATION REPORT NUMBER. Enter all unique alphanumeric report numbers assigned by the performing organization, e.g. BRL-1234; AFWL-TR-85-4017-Vol-21-PT-2.

9. SPONSORING/MONITORING AGENCY NAME(S) AND ADDRESS(ES). Enter the name and address of the organization(s) financially responsible for and monitoring the work.

10. SPONSOR/MONITOR'S ACRONYM(S). Enter, if available, e.g. BRL, ARDEC, NADC.

11. SPONSOR/MONITOR'S REPORT NUMBER(S). Enter report number as assigned by the sponsoring/ monitoring agency, if available, e.g. BRL-TR-829; -215.

12. DISTRIBUTION/AVAILABILITY STATEMENT. Use agency-mandated availability statements to indicate the public availability or distribution limitations of the report. If additional limitations/ restrictions or special markings are indicated, follow agency authorization procedures, e.g. RD/FRD, PROPIN, ITAR, etc. Include copyright information.

13. SUPPLEMENTARY NOTES. Enter information not included elsewhere such as: prepared in cooperation with; translation of; report supersedes; old edition number, etc.

14. ABSTRACT. A brief (approximately 200 words) factual summary of the most significant information.

15. SUBJECT TERMS. Key words or phrases identifying major concepts in the report.

16. SECURITY CLASSIFICATION. Enter security classification in accordance with security classification regulations, e.g. U, C, S, etc. If this form contains classified information, stamp classification level on the top and bottom of this page.

17. LIMITATION OF ABSTRACT. This block must be completed to assign a distribution limitation to the abstract. Enter UU (Unclassified Unlimited) or SAR (Same as Report). An entry in this block is necessary if the abstract is to be limited.